Extraordinary Interfacial Stitching between Single All-Inorganic Perovskite Nanocrystals

Gomez, L.; Lin, J.; de Weerd, C.; Poirier, L.; Boehme, S.C.; von Hauff, E.; Fujiwara, Y.; Suenaga, K.; Gregorkiewicz, T.

DOI
10.1021/acsami.7b17432

Publication date
2018

Document Version
Final published version

Published in
ACS Applied Materials and Interfaces

ACS APPLIED MATERIALS & INTERFACES

Research Article

Cite This: ACS Appl. Mater. Interfaces 2018, 10, 5984−5991

www.acsami.org

Extraordinary Interfacial Stitching between Single All-Inorganic Perovskite Nanocrystals

Leyre Gomez,*[,†] Junhao Lin,*[,‡] Chris de Weerd,[†] Lucas Poirier,[†] Simon C. Boehme,[∥] Elizabeth von Hauff,[∥] Yasufumi Fujiwara,[§] Kazutomo Suenaga,[‡] and Tom Gregorkiewicz[†]

[†]Institute of Physics, University of Amsterdam, Science Park 904, 1098 XH Amsterdam, The Netherlands

[‡]National Institute of Advanced Industrial Science and Technology (AIST), AIST Central 5, Tsukuba 305-8565, Japan

[§]Division of Materials and Manufacturing Science, Graduate School of Engineering, Osaka University, 2-1 Yamadaoka, Suita, Osaka 565-0871, Japan

[∥]Department of Physics and Astronomy, Vrije Universiteit Amsterdam, De Boelelaan 1081, 1081 HV Amsterdam, The Netherlands

Supporting Information

ABSTRACT: All-inorganic cesium lead halide perovskite nanocrystals are extensively studied because of their outstanding optoelectronic properties. Being of a cubic shape and typically featuring a narrow size distribution, $CsPbX_3$ (X = Cl, Br, and I) nanocrystals are the ideal starting material for the development of homogeneous thin films as required for photovoltaic and optoelectronic applications. Recent experiments reveal spontaneous merging of drop-casted $CsPbBr_3$ nanocrystals, which is promoted by humidity and mild-temperature treatments and arrested by electron beam irradiation. Here, we make use of atom-resolved annular dark-field imaging microscopy and valence electron energy loss spectroscopy in a state-of-the-art low-voltage monochromatic scanning transmission electron microscope to investigate the aggregation between individual nanocrystals at the atomic level. We show that the merging process preserves the elemental composition and electronic structure of $CsPbBr_3$ and takes place between nanocrystals of different sizes and orientations. In particular, we reveal seamless stitching for aligned nanocrystals, similar to that reported in the past for graphene flakes. Because the crystallographic alignment occurs naturally in drop-casted layers of $CsPbX_3$ nanocrystals, our findings constitute the essential first step toward the development of large-area nanosheets with band gap energies predesigned by the nanocrystal choice—the gateway to large-scale photovoltaic applications of inorganic perovskites.

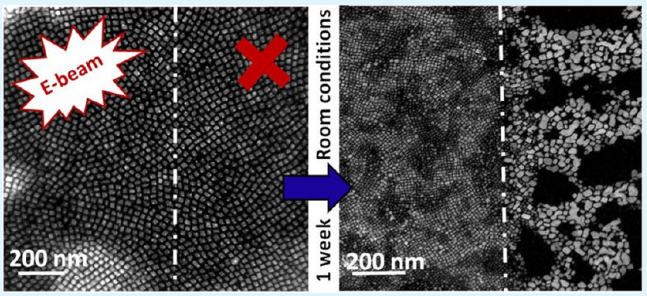

KEYWORDS: *inorganic perovskites, nanocrystals, seamless stitching, merging, EELS, high-resolution TEM*

1. INTRODUCTION

Metal halide semiconductors with a perovskite structure currently captivate much interest because of their attractive optical and electrical properties (broad range of band gap energy values, high emission efficiency, high carrier mobilities, and simple and low-cost synthesis). Most research effort is focused on hybrid organic−inorganic perovskites (e.g., $CH_3CH_3PbI_3$, $CH_3NH_3PbI_3$, etc.). For large-scale applications, in photovoltaics (PV) for instance, excellent long-term (chemical and structural) stability under operating conditions is an absolute necessity. However, this represents a considerable challenge for the hybrid perovskites.

Recently, the synthesis of all-inorganic cesium lead halide perovskite nanocrystals ($CsPbX_3$ with X = Cl, Br, and I; IP-NCs) has been developed.[1] This material combines the advantages of perovskites (low-temperature/low-cost production and band gap tuning by composition) with the typical NC characteristics induced by quantum confinement (band gap tuning by size, energy transfer, and a possibility of surface functionalization).[2,3] Furthermore, IP-NCs feature a high photoluminescence quantum yield (PL QY = 50−90%) and narrow emission bands with a tunability over the whole visible range.[4,5] At the same time, being free from any organic element, the IP-NCs are more stable than hybrid perovskites, which makes them attractive for PV as well as optoelectronic applications: solar cells, LEDs, lasers, and detectors.[6−9] Although IP-NCs allow for the engineering of electronic states, carrier interactions, and dynamics, their conductivity in quantum solids built of semiconductor NCs is typically rather poor because of the presence of a confining potential, which introduces a barrier for carrier transport. This serious disadvantage has prevented a broader application of semiconductor NCs for solar cells in the past. However, the recent demonstration of a stable solar cell based on $CsPbI_3$ NCs forming thin layers with superior electrical properties[9−11] offers a new hope. This development directly illustrates that to

Received: November 15, 2017
Accepted: January 22, 2018
Published: January 22, 2018

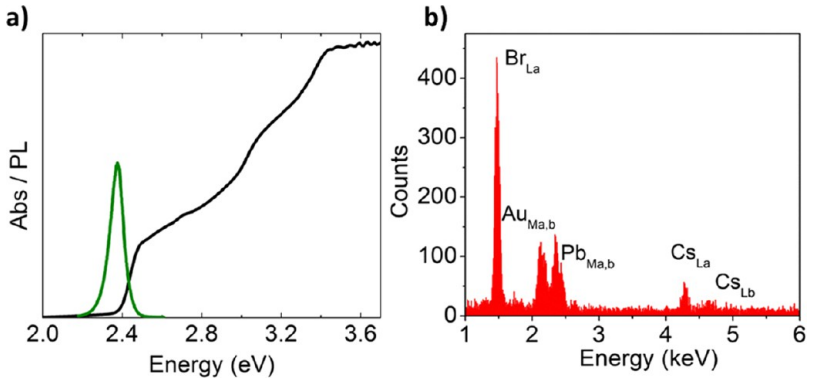

Figure 1. Optical spectroscopy and structural characterization of ensemble $CsPbBr_3$ NCs. (a) Absorption and PL spectra of colloidal NCs in toluene. (b) EDXS spectra confirming the ideal perovskite composition Cs:Pb:Br = 1:1:3 (integrated area under the respective peaks), without a notorious presence of Cs_4PbBr_6.[27]

fabricate a superior device based on NCs and in particular on IP-NCs, they need to form stable thin layers with good electrical contact between individual NCs of the highest quality.

The sintering of metal nanoparticles by different processes (high-temperature, pressure-driven, microwave or laser radiation, etc.),[12−15] even at room temperature,[16−18] has been investigated in the past. Similarly, aggregation of semiconductor NCs into 2D sheets has been reported.[19,20] Nevertheless, the spontaneous merging of IP-NCs passivated by long-alkyl chain ligands is considered as a structural instability[21,22] rather than the initial step for the formation of homogeneous thin layers—to the best of our knowledge. From our previous investigations of IP-NCs, we concluded that the effective coupling between proximal $CsPbBr_3$ NCs in an ensemble leads to their band structure modification[23] and to an efficient energy transfer.[24] Therefore, IP-NCs are excellent candidates for custom-designed quantum structures and solids which could be realized by purposeful assemblage of individually characterized and selected NCs serving as building blocks.[25] Because of their cubic shape and a narrow size distribution, IP-NCs are ideally suited to form close-packed layers and/or multilayer structures. Moreover, closely packed proximal IP-NCs merge together, forming larger structures. We conclude that IP-NCs with a high "defect tolerance"[26] could possibly be used for the development of thin films, which are highly attractive for solar cells and optoelectronic applications.

In the present work, we investigate the aggregation process of individual IP-NCs at the atomic scale. By using state-of-the-art annular dark-field (ADF) imaging and electron energy loss spectroscopy (EELS) in an aberration-corrected scanning transmission electron microscope (STEM), we show the microscopic details of the stitching between individual IP-NCs of different sizes and crystallographic orientations. This finding constitutes the first and the most essential step toward the development of high-quality thin films of IP-NCs, whose properties can be tuned by selecting appropriate NCs. More generally, the event of the well-controlled aggregation of NCs paves the way toward advanced concepts of purposeful assemblage of nano-objects into larger structures.

2. MATERIALS AND METHODS

2.1. Materials. Cesium carbonate (Cs_2CO_3 99.9%, Sigma-Aldrich), octadecene (ODE 90%, Sigma-Aldrich), oleic acid (OA 90%, Sigma-Aldrich), oleylamine (OLA 80−90%, Acros), lead(II) bromide ($PbBr_2$ 98%, Sigma-Aldrich), and toluene (ACS reagent ≥99.5%, Sigma-Aldrich) were used with no further purification, except for the drying period reported in the synthesis procedure.

2.2. Synthesis of $CsPbBr_3$ NCs. First, Cs-oleate was prepared by the reaction of 814 mg of Cs_2CO_3 with 40 mL of ODE and 2.5 mL of OA at 150 °C; the reactants were previously dehydrated for 1 h at 120 °C. For the production of $CsPbBr_3$ NCs, 30 mL of ODE and 700 mg of $PbBr_2$ were dried for 1 h at 120 °C under a N_2 atmosphere. After water removal, 5 mL of dried OLA and 5 mL of dried OA were added to the reaction flask, and the temperature was raised up to 160 °C. After complete solvation of the $PbBr_2$ salt, 4 mL of Cs-oleate solution previously warmed was injected. A few seconds later, the NC solution was quickly cooled down with an ice bath. The product was purified by repeated centrifugation and redispersion in toluene.

2.3. Merging Experiments. We drop-casted the IP-NC samples on amorphous carbon/graphene TEM grids and stored them at room conditions for the spontaneous merging of NCs to occur. Room conditions refer to a typical ambient environment with moderate humidity. To probe the effect of humidity, we drop-casted the same amount of colloidal NC solution onto two identical grids and stored them separately under lower (∼20%) and higher (∼60%) relative humidity (RH) conditions, at room temperature. To test the effect of temperature, we used a cooling or heating in situ sample holder (Gatan) to reach the temperature ranges between −110 °C to 90 °C and 90 °C to 260 °C, respectively. The electron beam-irradiated samples/areas were exposed to the electron beam directly after drop-casting and subsequent cooling or heating.

For the electrical measurements, the films were fabricated by drop-casting the NC dispersion onto Au-interdigitated electrodes with a 5 μm channel width (DropSens G-IDEAU5). Immediately before drop-casting, the electrodes were electrochemically cleaned in H_2SO_4.

2.4. Characterization. The optical density was measured in a LAMBDA 950 UV/VIS/NIR spectrophotometer (PerkinElmer). A combination of tungsten-halogen and deuterium lamps was used together with PMT and Peltier-cooled PbS detectors, to provide a detection range of E_{det} = 0.4−5.6 eV. For reference, the absorption of the solvent was measured separately and subsequently subtracted from that of the colloid dispersion.

The PL spectra were recorded using a Jobin Yvon FluoroLog spectrofluorometer (Horiba) equipped with a 450 W xenon lamp (250−700 nm) coupled to a monochromator to provide a range of selective excitation wavelengths. The emission was collected in right-angle geometry and automatically corrected for the spectral sensitivity of the setup. To determine the PL QY, the samples were placed in an integrating sphere, using a 150 W xenon lamp coupled to a spectrometer (Solar, MSA-130) as an excitation source. The PL emission and excitation lights were scattered diffusively in the integrating sphere and were detected by a CCD (Hamamatsu).

Scanning transmission electron microscopy (STEM)−EELS spectra were obtained in a low-voltage JEOL-2100F with a double delta corrector, which has a probe size of around 1.4 Å, and in a low-voltage JEOL-ARM60 with a double Wien filter monochromator offering an

DOI: 10.1021/acsami.7b17432
ACS Appl. Mater. Interfaces 2018, 10, 5984−5991

ultrahigh spatial and energy resolutions of around 1.4 Å and 50 meV, respectively. Current−voltage measurements were performed at a scan rate of 47 mV/s, with a Keithley 2400 source meter and a home-made LabVIEW program.

Frequency-resolved electrical measurements were performed in the dark, at a bias voltage of 0 V and an ac amplitude of 20 mV, using a Metrohm-Autolab electrochemical impedance spectroscopy setup (PGSTAT302N) equipped with a FRA32M module.

3. PRELIMINARIES

The synthesis of $CsPbBr_3$ NCs was carried out following the protocol reported by Protesescu et al.,[1] which was slightly modified. The green-emitting perovskites, stabilized with OLA and OA on their surface, show a narrow emission band centered at 520 nm (2.38 eV), with a small Stokes shift from the corresponding absorption spectrum (Figure 1a). Figure 1b shows the energy-dispersive X-ray spectrometry (EDXS) spectrum indicating the presence of Cs, Pb, and Br in a 1:1:3 ratio, hence confirming the perovskite ABX_3 elemental composition.[27] A fresh sample, drop-casted on an amorphous carbon/graphene grid, reveals the presence of cubic IP-NCs with a narrow size distribution of 8.1 ± 1.2 nm (Figure 2a).

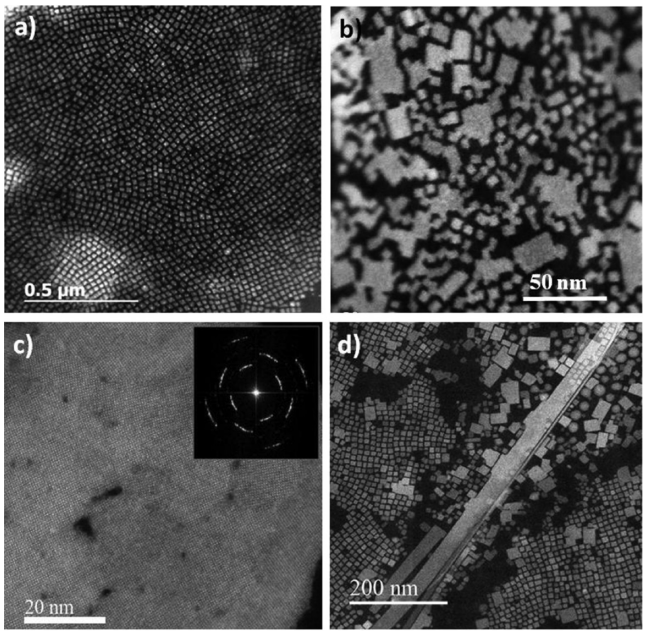

Figure 2. ADF−STEM images of drop-casted $CsPbBr_3$ NCs on an amorphous carbon/graphene grid. (a) Fresh drop-casted sample. (b) Same sample after being stored at room conditions for a week. (c) Another region of merged NCs; the inset shows the fast Fourier transformation pattern, demonstrating the misorientation from different small domains. (d) Sample stored at room conditions for 6 months.

The NCs arrange themselves in ordered square geometries, in some analogy to the honeycomb superlattices of PbSe NCs.[28] Despite being clearly separated by surface ligand layers, neighboring IP-NCs effectively couple, modifying the energy structure of each other.[23] When stored at room conditions, the NC layer spontaneously aggregates, with individual IP-NCs merging into larger structures (Figure 2b). Eventually, after a sufficiently long time, a semicontinuous layer of rather poor homogeneity is formed (Figure 2c). In the case of a NC layer of low density, isolated nanoplatelets appear. When the storage time is increased to 6 months (Figure 2d), the NCs can arrange in very long nanowires (aspect ratios of ∼100 and higher), although individual NCs are still visible; to grow a large homogenous film of merged NCs, other parameters (humidity, temperature, etc.) should be considered as we will reveal along this paper. We have observed this aggregation process in the layers of IP-NCs of different sizes and chemical compositions. It is important to note that upon merging, their chemical composition is maintained (see Figure S1 of the Supporting Information), which implies that no chemical reactions are involved and that larger IP platelets are created. At the same time, we observe that the merging of individual IP-NCs changes the optical properties of a layer, red-shifting its PL spectrum and absorption edge. We evaluated this effect using a drop-casted layer of $CsPbBr_3$ NCs on a quartz substrate (Figure S2). In addition, the merging process leads to a reduction of the PL QY (Figure S3). The effect of exposure to light and air on the NC aggregation has also been observed (Figures S4). The sample stored for 1 week in the dark in an inert gas atmosphere exhibited a negligible change in the PL QY, whereas the sample stored in air while being constantly illuminated showed a major QY decrease, by a factor of 6.[21]

Also, the electrical properties are influenced by the merging. To investigate that, we drop-casted IP-NCs on interdigitated electrodes (5 μm width) and measured the current−voltage characteristics after 1 h, 1 day, and 9 days of storage in air (see Figure S5). We note that while the fresh drop-casted film is conductive, the NC aggregation increases its resistivity, as the merging of individual IP-NCs into larger clusters leads to the formation of voids, which disrupt the percolative pathways across the 5 μm distance between the electrodes. This problem could possibly be addressed by adding successive layers of NCs to fill in those voids.

4. MICROSCOPIC INVESTIGATIONS AND DISCUSSION

To understand the merging process of IP-NCs in some detail, we performed experiments at a microscopic level. For that purpose, a $CsPbBr_3$ NC dispersion in toluene has been drop-casted on an amorphous carbon/graphene TEM grid for high-resolution ADF−STEM imaging.

We start the investigation comparing the EELS spectra of fresh drop-casted (Figure 3a) and merged (Figure 3b) IP-NCs. Using EELS, it is possible to measure the band-to-band absorption of individual NCs. The EELS spectrum shows a characteristic onset, which arises from the excitation of a valence band electron to the conduction band, defining the band gap energy.[23] For a fresh drop-casted film, before merging, the accumulated EELS signal measured at different points of the layer represents the sum of the (averaged) absorption by neighboring NCs. The EELS spectra showing the measurements collected at different points for the fresh drop-casted NC layer and for the semiuniform film formed by merging are presented in Figure 3c. The EELS data for both configurations feature a similar absorption behavior, with the characteristic onset at the band gap energy, in analogy to the optical density of a bulk semiconductor. Comparing the two spectra, the band gap energy slightly red-shifts (∼60 meV) upon merging (E_{fresh} = 2.45 eV and E_{merged} = 2.39 eV), approaching the bulk value[29] (E_{bulk} = 2.32 eV). We note that the aggregated IP film still exhibits a small quantum confinement induced by its nanometer-range thickness.[23]

Subsequently, we zoom-in to reveal more details of the merging between individual IP-NCs. Figure 4a shows a high-resolution ADF−STEM image of a dense layer of fresh drop-

DOI: 10.1021/acsami.7b17432
ACS Appl. Mater. Interfaces 2018, 10, 5984−5991

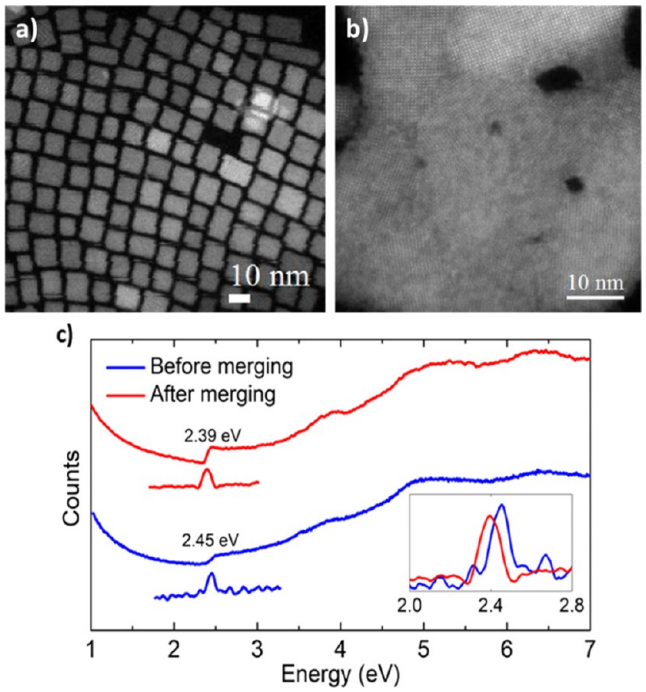

Figure 3. Comparison of the absorption of a fresh drop-casted sample and a 1 week old region of the film, investigated by EELS. (a) ADF–STEM image of the fresh drop-casted $CsPbBr_3$ NCs. (b) Similar but different region (unexposed to the electron beam) of the sample after 1 week of storage at room conditions after which the NCs have merged. (c) Local low-loss (LL)-EELS spectra averaged over the regions shown in panels a (blue spectrum) and b (red spectrum), with the band gap energy values extracted from their first derivatives, 2.45 and 2.39 eV, respectively.

casted NCs. For some NCs, linear defects can be distinguished, as indicated by the arrows; these could indicate the NC growth process. The merging process is very evident when we inspect the film that was stored for a week. Figure 4b,c shows that the aggregation process connects NCs not only of the same but also of a different orientation and that the size of joining NCs does not seem to play a role. A more careful inspection of the images reveals that the new structures appear to be of high crystallinity, without borders between the merging NCs (Figure 4b), whereas for some connecting NCs, clear boundaries are present (Figure 4c).

The ultimate illustration of the aggregation process is provided by imaging at a single-NC level. Figure 5a shows a large IP-NC, with the edge exceeding 50 nm. For reference, also a 6 nm edge size NC from the originally drop-casted layer is shown (Figure 5b). We conclude that in this case, the merge is ideal, creating an apparently monocrystalline structure throughout the whole cluster. A similar seamless stitching has been reported before for graphene flakes, in which case, the mutual orientation of the individual flakes was crucial.[30] Here, the necessary alignment of individual IP-NCs with respect to each other is conveniently facilitated by spontaneous formation of the square superlattice in the drop-casted layer (see Figure 3a). Figure 5 also illustrates that, as noticed already before, merging of individual NCs can also occur in other configurations, with a tilted angle (Figure 5c,d) or with a different zone axis (Figure 5e). Therefore, we conclude that the stitching can occur between all neighboring NCs, independently of their sizes and orientations. This random stitching could be advantageous because it means that all neighboring NCs will fuse, creating a continuous thin perovskite film. A noncrystalline surface layer, which we identify with the stabilizing ligands, can be observed around the newly formed structures. This implies that the ligands do not disappear upon merging but merely relocate, increasing the amount of hydrocarbon chains at the edge of the larger assemblies. We conclude that the growth of clusters and also the subsequent development of large structures, such as long nanowires and extensive semicontinuous thin films of IP-NCs, proceed by sequential merging of individual NCs and not by, for example, Ostwald ripening, as the NCs merge together and not gradually dissolve in one another.

Although the formation of perfectly uniform and crystalline large structures is possible by seamless stitching, as illustrated in Figure 5, in general, the merged IP-NC film can be viewed as a large plate with numerous smaller and larger (mono)crystalline domains formed by aggregation, with their grain boundaries containing multiple structural imperfections (Figure 2c).[31] Using the superior spatial resolution of EELS, we can now investigate the effect of these grain-boundary-related defects on the electronic band structure of the film. To achieve that, we select a particular "imperfectly" merged cluster (with clear boundaries between connecting NCs) and monitor the EELS spectrum as we scan the electron beam between individual grains, across the interface. The experiment shows that the absorption spectra obtained by the locally conducted EELS are practically identical over the whole investigated trajectory within the IP cluster. This is illustrated in Figure 6, which compares three different spectra taken in the middle of the two adjacent grains and at their interface; a very close similarity is evident. Moreover, we notice that the EELS measurements of the merged film yield spectra that are practically unaltered from

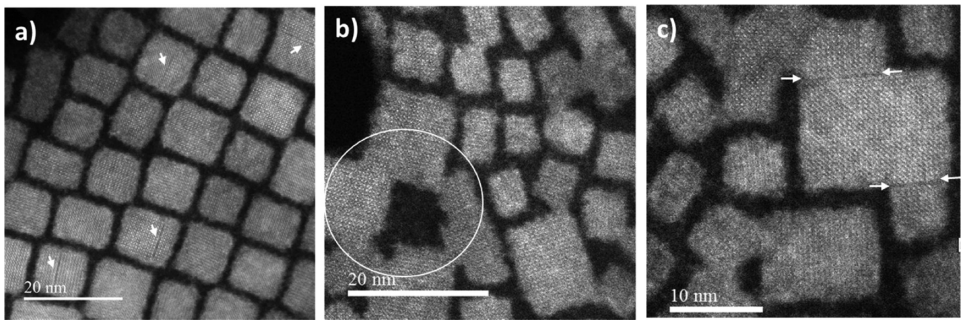

Figure 4. High-resolution images of a dense layer of $CsPbBr_3$ NCs. (a) Line defects are found in some NCs, identified with arrows. (b) Connected NCs share the same orientation, in this case, along the [001] direction. (c) Boundaries at the connections are clearly visualized.

DOI: 10.1021/acsami.7b17432
ACS Appl. Mater. Interfaces 2018, 10, 5984–5991

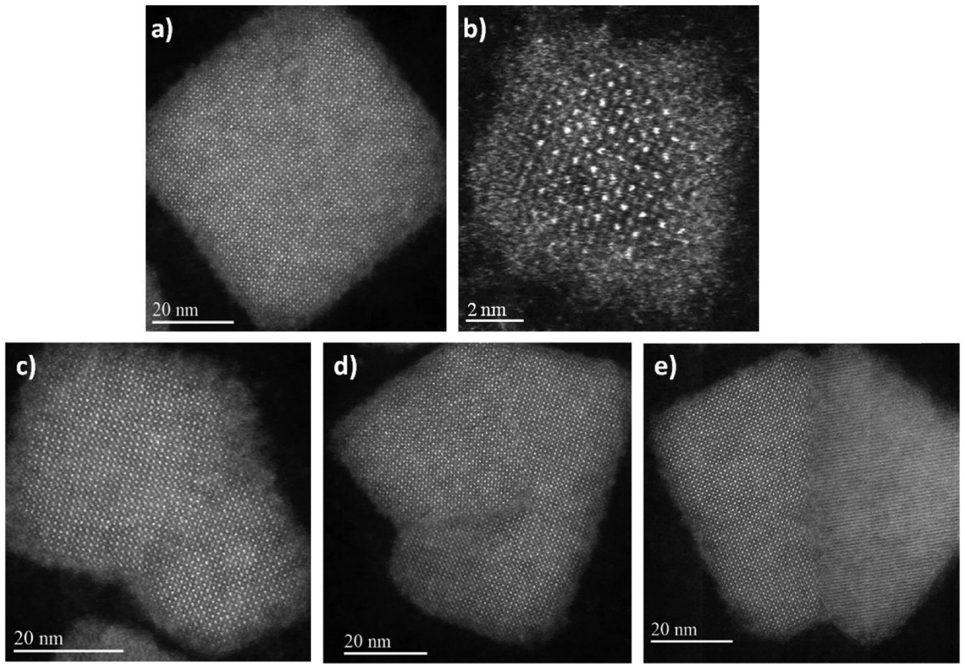

Figure 5. High-resolution ADF–STEM images of single and merged IP-NCs. (a) Large $CsPbBr_3$ NC made by the merging of small NCs. (b) Original NC synthesized by wet chemistry. (c) NCs merged with the same crystal orientation but a different tilting angle. (d) Small and large NCs merged with a different tilting angle. (e) Two NCs of a similar size merged with a different zone axis.

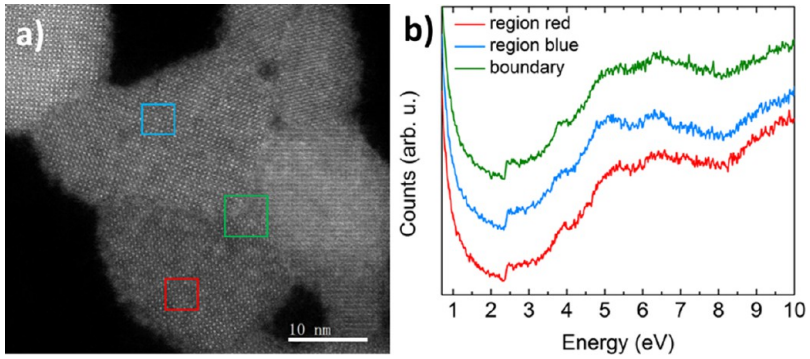

Figure 6. EELS scan across the boundaries between merged NCs. (a) ADF image of merged $CsPbBr_3$ NCs with visible boundaries and (b) their corresponding EELS spectra. There is no noticeable difference in the absorption behavior and band gap energy observed, where the boundary of merged NCs (green) and a smooth part of the film (blue and red) are compared.

those of individual IP-NCs which we reported previously.[23] A particularly striking feature is that the interface apparently does not introduce significant amounts of defects in the band gap nor disturbs the band structure close to the band edges. This implies that even the obviously imperfect boundary arising upon layer formation does not yield defects which would strongly influence the transport properties of the film and its performance in a solar cell (see also Figure S6). This truly microscopic finding is essential for the photovoltaic potential of IP layers created by aggregation of NCs. In the broader context of all perovskite materials currently vividly explored for solar cells, this finding provides also an important clue concerning the microscopic origin of the good mobilities and apparent defect tolerance of these materials. We conclude that the spontaneous orderly aggregation of IP-NCs offers a unique opportunity to create nanosheets (nanometer thick IP layers exhibiting quantum confinement-related effects) whose characteristics can be predefined (tuned) by the properties of the used IP-NCs. In the future, the deposition of IP-NC layers could be conveniently controlled by jetting.[32,33]

Having established the microscopic formation mechanism of IP nanosheets and their remarkable characteristics, we turn our attention to the practical aspects of the merging process. In general, the self-assembly of NCs drop-casted or spin-coated on a substrate from a colloidal solution is governed by interactions between the NCs and with the substrate, solution/substrate interface, drying kinetics (solvent- and temperature-dependent), among others.[34−36] The contact between colloidal semiconductor NCs themselves is facilitated by van der Waals forces, which are weak and can easily be overcome by steric repulsions using stabilizing ligands.[37] Nevertheless, the highly dynamic behavior of the IP-NC surface ligands (the binding is not strong, and they can move and be easily lost, mainly during the purification process) besides the ionic character of the IP-NC structure makes this material breakable in polar solvents.[38] These characteristics are important for manipulating and eventually controlling the assemblage of IP-NCs. In the

DOI: 10.1021/acsami.7b17432
ACS Appl. Mater. Interfaces 2018, 10, 5984−5991

following section, we present how electron bean irradiation, humidity, and thermal annealing at different temperatures influence the aggregation process.

Electron irradiation can affect the ligands that are present at the surface of the deposited IP-NCs, leading to the formation of intermolecular C═C bonds between them and also between the ligands and the carbonaceous grid;[39] in both cases, the IP-NC stability would be enhanced. This is indeed confirmed in our experiments: Figure 7a,b shows the images of drop-casted

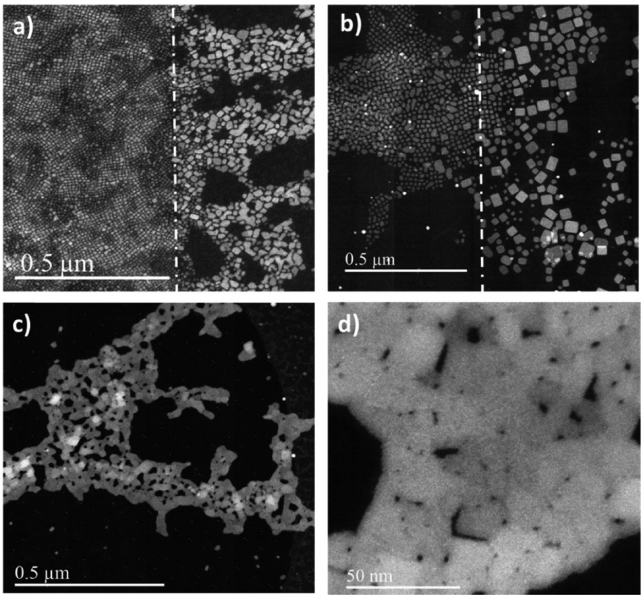

Figure 7. Influence of electron beam irradiation and mild-temperature annealing on the IP-NCs merging. (a) One week-aged high-IP-NCs density layer sample, being partially irradiated with electrons just after deposition—left side of the image, and without previous irradiation—right side of the iamge. (b) Lower IP-NCs density layer annealed at 90 °C for 1 h, being partially irradiated with electrons just after deposition—left side of the image, and no previous irradiation—right side of the image. (c) IP-NCs annealed at 90 °C for 1 h without previous electron irradiation. (d) Zoom-in of the sample in c.

IP-NC stored for 1 week at room conditions; the left part is exposed to an electron beam directly after deposition, whereas the right-hand side is not. As can be seen, the NC aggregation has taken place only in the nonirradiated part of the sample, thus illustrating the stabilizing action of the electron beam.

Typically, aggregation processes are strongly temperature-dependent, and this is also the case for the IP-NC layers, with their merging being accelerated by mild-temperature treatments due to the removal of surface ligands.[21] At the macroscopic level, this is evidenced by the fact that IP-NC films on quartz treated at mild temperatures show a decrease of the emission intensity and PL QY because of the defect formation (see Figure S7), in agreement with previous reports.[21,40] Here, we investigate this effect at the microscopic level. Figure 7b shows the behaviors of electron-irradiated and nonirradiated regions of a low-concentration IP-NC layer, annealed at 90 °C for 1 h. Whereas the NCs in the electron-irradiated region remain isolated, the merging process in the untreated part of the sample is clearly enhanced. When the initial NC density is high, the same treatment results in a complete fusion of individual NCs into a semicontinuous film (Figure 7c,d). For the development of high-quality layers, the annealing temperature will need to be optimized, as high-temperature treatments destroy the IP-NCs (see Figure S8). In Figure 8a, small clusters of 14 NCs are imaged directly after drop-casting; an amorphous

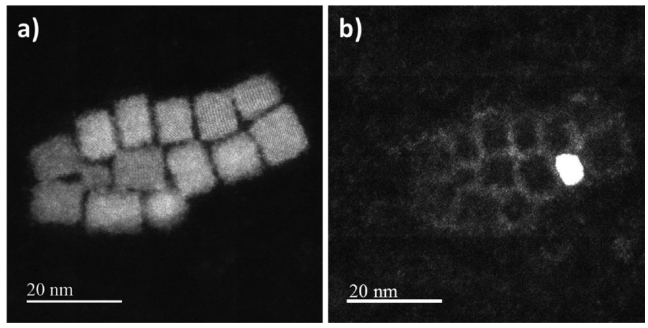

Figure 8. Effect of annealing IP-NCs at a high temperature. (a) ADF–STEM image of 14 $CsPbBr_3$ NCs. (b) Same IP-NCs after 1 h of annealing treatment at 260 °C; just remaining the residual ligands and a metallic nanoparticle (bright dot).

layer of ligands is clearly visible on the individual NC surface. The electron irradiation stabilizes the ligands, as discussed before, arresting the possible merging. Figure 8b shows the same cluster after being heated at 260 °C for 1 h: the IP-NCs have been completely destroyed, with a small metallic nanoparticle being formed from the IP-NC debris, whereas the residual shell of ligands remains, now around the empty spaces.

Past research has shown that ethanol influences the growth of IP-NCs through surface ligand destabilization[41] and can induce partial dissolution and subsequent recrystallization of IP-NCs—the effect which can serve for healing of the film.[42] To investigate the effect of water vapor on the NC merging, we compared two samples stored for 1 week in dry (RH = 20%) and high-humidity atmospheres (RH = 60%). The results (Figure 9) clearly show that the water vapor accelerates the NC

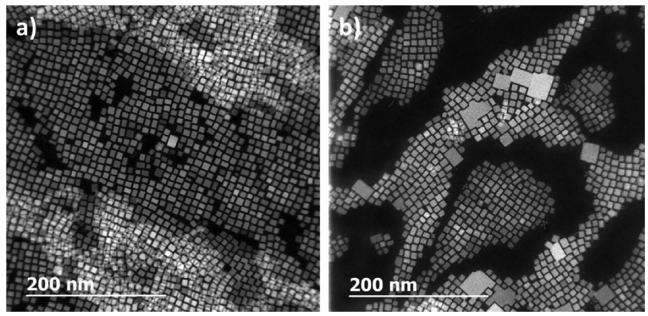

Figure 9. Effect of the RH on the merging of IP-NCs. ADF–STEM images of drop-casted $CsPbBr_3$ NCs stored for 1 week in (a) a vacuum chamber with RH = 20% and (b) in a humidifier with RH = 60%.

fusion process. Because water actually dissolves the perovskites and in that way destroys the IP-NCs, specific investigations are necessary to determine the optimal RH level for the merging process, similarly as for the thermal treatment.

5. CONCLUSIONS

Colloidal IP-NCs drop-casted on a substrate form spontaneously a semihomogeneous thin film. A thorough microscopic investigation by our state-of-the-art ADF microscopy and EELS reveals that the layer formation proceeds by merging of individual NCs. We show that the fusion is accelerated by mild-

DOI: 10.1021/acsami.7b17432
ACS Appl. Mater. Interfaces 2018, 10, 5984–5991

temperature annealing in a humid atmosphere. Surface ligands play an active role in the aggregation process, which is arrested or totally prevented by their stabilization, for example, upon electron irradiation. Most importantly, at the atomic level, we find that the merging process does not introduce an appreciable defect concentration in the band gap or at the band edges, and even near-perfect seamless stitching between the aligned NCs is possible. Because crystallographic alignment naturally arises in drop-casted dense layers of IP-NCs, this implies that in the future, this process could be explored for formation of thin IP films of superior quality. Our results demonstrate the fundamental condition growth for the development of these sheets, the seamless stitching; future research must show whether it is also "sufficient"; that is, if it can be extended to grow long thin films. In that way, the current findings certify the high potential of IP-NCs for practical applications in future thin-film PV. In a broader context, they pave the way toward dedicated engineering of high-quality thin IP films, creating custom-designed quantum structures by purposeful assemblage of individually characterized and selected NCs.

■ ASSOCIATED CONTENT

Supporting Information

The Supporting Information is available free of charge on the ACS Publications website at DOI: 10.1021/acsami.7b17432.

EDXS and EELS of individual nanocrystals, impedance spectroscopy, additional ADF−TEM images, and quantum efficiency data (PDF)

■ AUTHOR INFORMATION

Corresponding Authors

*E-mail: L.gomeznavascues@uva.nl (L.G.).
*E-mail: lin.junhao@aist.go.jp (J.L.).

ORCID

Leyre Gomez: 0000-0002-2926-5665
Junhao Lin: 0000-0002-2195-2823
Chris de Weerd: 0000-0002-8826-2616
Elizabeth von Hauff: 0000-0002-6269-0540
Tom Gregorkiewicz: 0000-0003-2092-8378

Author Contributions

L.G. and J.L. contributed equally to this work. L.G., J.L., K.S., and T.G. conceived the project and designed the experiments. L.G. prepared the samples. J.L. performed the LL-EELS measurements and analyzed the data. C.d.W. and L.P. performed the optical spectroscopy measurements and analyzed the data. E.v.H. and S.C.B. performed the electrical experiments. All authors discussed the results and their interpretation. L.G., J.L., and C.d.W. cowrote the manuscript with contributions from K.S. and T.G. who also cosupervised the project with Y.F.

Notes

The authors declare no competing financial interest.

■ ACKNOWLEDGMENTS

C.d.W., L.G., and T.G. acknowledge the Dutch Technology Foundation STW, which is part of the Netherlands Organisation for Scientific Research (NWO) for financial support. J.L. and K.S. work has been financed by JST-ACCEL and JSPS KAKENHI (JP16H06333 and P16823). E.v.H. thanks the Foundation for Fundamental Research on Matter (FOM) (V0714M-13MV60) from the Netherlands Organization for Scientific Research (NWO) for funding. Y.F. and T.G. thank Osaka University for International Joint Research Promotion Program.

■ REFERENCES

(1) Protesescu, L.; Yakunin, S.; Bodnarchuk, M. I.; Krieg, F.; Caputo, R.; Hendon, C. H.; Yang, R. X.; Walsh, A.; Kovalenko, M. V. Nanocrystals of cesium lead halide perovskites ($CsPbX_3$, X = Cl, Br, and I): novel optoelectronic materials showing bright emission with wide color gamut. *Nano Lett.* **2015**, *15*, 3692−3696.

(2) Kazim, S.; Nazeeruddin, M. K.; Grätzel, M.; Ahmad, S. Perovskite as light harvester: a game changer in photovoltaics. *Angew. Chem., Int. Ed.* **2014**, *53*, 2812−2824.

(3) Bawendi, M. G.; Steigerwald, M. L.; Brus, L. E. The quantum mechanics of larger semiconductor clusters ("quantum dots"). *Annu. Rev. Phys. Chem.* **1990**, *41*, 477−496.

(4) Wei, S.; Yang, Y.; Kang, X.; Wang, L.; Huang, L.; Pan, D. Room-temperature and gram-scale synthesis of $CsPbX_3$ (X = Cl, Br, I) perovskite nanocrystals with 50−85% photoluminescence quantum yields. *Chem. Commun.* **2016**, *52*, 7265−7268.

(5) Chen, X.; Peng, L.; Huang, K.; Shi, Z.; Xie, R.; Yang, W. Non-injection gram-scale synthesis of cesium lead halide perovskite quantum dots with controllable size and composition. *Nano Res.* **2016**, *9*, 1994−2006.

(6) Yakunin, S.; Protesescu, L.; Krieg, F.; Bodnarchuk, M. I.; Nedelcu, G.; Humer, M.; De Luca, G.; Fiebig, M.; Heiss, W.; Kovalenko, M. V. Low-threshold amplified spontaneous emission and lasing from colloidal nanocrystals of caesium lead halide perovskites. *Nat. Commun.* **2015**, *6*, 8056.

(7) Palazon, F.; Di Stasio, F.; Akkerman, Q. A.; Krahne, R.; Prato, M.; Manna, L. Polymer-free films of inorganic halide perovskite nanocrystals as UV-to-white color-conversion layers in LEDs. *Chem. Mater.* **2016**, *28*, 2902−2906.

(8) Ramasamy, P.; Lim, D.-H.; Kim, B.; Lee, S.-H.; Lee, M.-S.; Lee, J.-S. All-inorganic cesium lead halide perovskite nanocrystals for photodetector applications. *Chem. Commun.* **2016**, *52*, 2067−2070.

(9) Zeng, Q.; Zhang, X.; Feng, X.; Lu, S.; Chen, Z.; Yong, X.; Redfern, S. A. T.; Wei, H.; Wang, H.; Zheng, W.; Zhang, H.; Tse, J. S.; Yang, B. Polymer-passivated inorganic cesium lead mixed-halide perovskites for stable and efficient solar sells with high open-circuit voltage over 1.3 V. *Adv. Mater.* **2018**, 1705393.

(10) Swarnkar, A.; Marshall, A. R.; Sanehira, E. M.; Chernomordik, B. D.; Moore, D. T.; Christians, J. A.; Chakrabarti, T.; Luther, J. M. Quantum dot−induced phase stabilization of α-$CsPbI_3$ perovskite for high-efficiency photovoltaics. *Science* **2016**, *354*, 92−95.

(11) Sanehira, E. M.; Marshall, A. R.; Christians, J. A.; Harvey, S. P.; Ciesielski, P. N.; Wheeler, L. M.; Schulz, P.; Lin, L. Y.; Beard, M. C.; Luther, J. M. Enhanced mobility $CsPbI_3$ quantum dot arrays for record-efficiency, high-voltage photovoltaic cells. *Sci. Adv.* **2017**, *3*, No. eaao4204.

(12) Perelaer, J.; Klokkenburg, M.; Hendriks, C. E.; Schubert, U. S. Microwave flash sintering of inkjet-printed silver tracks on polymer substrates. *Adv. Mater.* **2009**, *21*, 4830−4834.

(13) Baumgardner, W. J.; Choi, J. J.; Bian, K.; Kourkoutis, L. F.; Smilgies, D.-M.; Thompson, M. O.; Hanrath, T. Pulsed laser annealing of thin films of self-assembled nanocrystals. *ACS Nano* **2011**, *5*, 7010−7019.

(14) Garnett, E. C.; Cai, W.; Cha, J. J.; Mahmood, F.; Connor, S. T.; Christoforo, M. G.; Cui, Y.; McGehee, M. D.; Brongersma, M. L. Self-limited plasmonic welding of silver nanowire junctions. *Nat. Mater.* **2012**, *11*, 241−249.

(15) Teulle, A.; Bosman, M.; Girard, C.; Gurunatha, K. L.; Li, M.; Mann, S.; Dujardin, E. Multimodal plasmonics in fused colloidal networks. *Nat. Mater.* **2015**, *14*, 87−94.

(16) Grouchko, M.; Kamyshny, A.; Mihailescu, C. F.; Anghel, D. F.; Magdassi, S. Conductive inks with a "built-in" mechanism that enables sintering at room temperature. *ACS Nano* **2011**, *5*, 3354−3359.

DOI: 10.1021/acsami.7b17432
ACS Appl. Mater. Interfaces 2018, 10, 5984−5991

(17) Grouchko, M.; Roitman, P.; Zhu, X.; Popov, I.; Kamyshny, A.; Su, H.; Magdassi, S. Merging of metal nanoparticles driven by selective wettability of silver nanostructures. *Nat. Commun.* **2014**, *5*, 2994.
(18) Aabdin, Z.; Lu, J.; Zhu, X.; Anand, U.; Loh, N. D.; Su, H.; Mirsaidov, U. Bonding pathways of gold nanocrystals in solution. *Nano Lett.* **2014**, *14*, 6639−6643.
(19) Schliehe, C.; Juarez, B. H.; Pelletier, M.; Jander, S.; Greshnykh, D.; Nagel, M.; Meyer, A.; Foerster, S.; Kornowski, A.; Klinke, C.; Weller, H. Ultrathin PbS sheets by two-dimensional oriented attachment. *Science* **2010**, *329*, 550−553.
(20) Ling, X.; Lin, Y.; Ma, Q.; Wang, Z.; Song, Y.; Yu, L.; Huang, S.; Fang, W.; Zhang, X.; Hsu, A. L.; Bie, Y.; Lee, Y.-H.; Zhu, Y.; Wu, L.; Li, J.; Jarillo-Herrero, P.; Dresselhaus, M.; Palacios, T.; Kong, J. Parallel stitching of 2D materials. *Adv. Mater.* **2016**, *28*, 2322−2329.
(21) Palazon, F.; Di Stasio, F.; Lauciello, S.; Krahne, R.; Prato, M.; Manna, L. Evolution of $CsPbBr_3$ nanocrystals upon post-synthesis annealing under an inert atmosphere. *J. Mater. Chem. C* **2016**, *4*, 9179−9182.
(22) Woo, J. Y.; Kim, Y.; Bae, J.; Kim, T. G.; Kim, J. W.; Lee, D. C.; Jeong, S. Highly stable cesium lead halide perovskite nanocrystals through in situ lead halide inorganic passivation. *Chem. Mater.* **2017**, *29*, 7088−7092.
(23) Lin, J.; Gomez, L.; de Weerd, C.; Fujiwara, Y.; Gregorkiewicz, T.; Suenaga, K. Direct observation of band structure modifications in nanocrystals of $CsPbBr_3$ perovskite. *Nano Lett.* **2016**, *16*, 7198−7202.
(24) de Weerd, C.; Gomez, L.; Zhang, H.; Buma, W. J.; Nedelcu, G.; Kovalenko, M. V.; Gregorkiewicz, T. Energy transfer between inorganic perovskite nanocrystals. *J. Phys. Chem. C* **2016**, *120*, 13310−13315.
(25) Hanrath, T. Colloidal nanocrystal quantum dot assemblies as artificial solids. *J. Vac. Sci. Technol., A* **2012**, *30*, 030802.
(26) Huang, H.; Bodnarchuk, M. I.; Kershaw, S. V.; Kovalenko, M. V.; Rogach, A. L. Lead halide perovskite nanocrystals in the research spotlight: stability and defect tolerance. *ACS Energy Lett.* **2017**, *2*, 2071−2083.
(27) de Weerd, C.; Lin, J.; Gomez, L.; Fujiwara, Y.; Suenaga, K.; Gregorkiewicz, T. Hybridization of single nanocrystals of Cs_4PbBr_6 and $CsPbBr_3$. *J. Phys. Chem. C* **2017**, *121*, 19490−19496.
(28) Boneschanscher, M. P.; Evers, W. H.; Geuchies, J. J.; Altantzis, T.; Goris, B.; Rabouw, F. T.; van Rossum, S. A. P.; van der Zant, H. S. J.; Siebbeles, L. D. A.; van Tendeloo, G.; Swart, I.; Hilhorst, J.; Petukhov, A. V.; Bals, S.; Vanmaekelbergh, D. Long-range orientation and atomic attachment of nanocrystals in 2D honeycomb superlattices. *Science* **2014**, *344*, 1377−1380.
(29) Kulbak, M.; Cahen, D.; Hodes, G. How important is the organic part of lead halide perovskite photovoltaic cells? Efficient CsPbBr3 cells. *J. Phys. Chem. Lett.* **2015**, *6*, 2452−2456.
(30) Nguyen, V. L.; Shin, B. G.; Duong, D. L.; Kim, S. T.; Perello, D.; Lim, Y. J.; Yuan, Q. H.; Ding, F.; Jeong, H. Y.; Shin, H. S.; Lee, S. M.; Chae, S. H.; Vu, Q. A.; Lee, S. H.; Lee, Y. H. Seamless stitching of graphene domains on polished copper (111) foil. *Adv. Mater.* **2015**, *27*, 1376−1382.
(31) Lee Penn, R.; Banfield, J. F. Imperfect oriented attachment: dislocation generation in defect-free nanocrystals. *Science* **1998**, *281*, 969−971.
(32) Perelaer, J.; Smith, P. J.; Mager, D.; Soltman, D.; Volkman, S. K.; Subramanian, V.; Korvink, J. G.; Schubert, U. S. Printed electronics: the challenges involved in printing devices, interconnects, and contacts based on inorganic materials. *J. Mater. Chem.* **2010**, *20*, 8446−8453.
(33) Song, J.; Xu, L.; Li, J.; Xue, J.; Dong, Y.; Li, X.; Zeng, H. Monolayer and few-layer all-inorganic perovskites as a new family of two-dimensional semiconductors for printable optoelectronic devices. *Adv. Mater.* **2016**, *28*, 4861−4869.
(34) Bishop, K. J. M.; Wilmer, C. E.; Soh, S.; Grzybowski, B. A. Nanoscale forces and their uses in self-assembly. *Small* **2009**, *5*, 1600−1630.
(35) Tang, J.; Ge, G.; Brus, L. E. Gas-liquid-solid phase transition model for two-dimensional nanocrystal self-assembly on graphite. *J. Phys. Chem. B* **2002**, *106*, 5653−5658.
(36) Rabani, E.; Reichman, D. R.; Geissler, P. L.; Brus, L. E. Drying-mediated self-assembly of nanoparticles. *Nature* **2003**, *426*, 271−274.
(37) Evers, W. H.; De Nijs, B.; Filion, L.; Castillo, S.; Dijkstra, M.; Vanmaekelbergh, D. Entropy-driven formation of binary semiconductor-nanocrystal superlattices. *Nano Lett.* **2010**, *10*, 4235−4241.
(38) De Roo, J.; Ibáñez, M.; Geiregat, P.; Nedelcu, G.; Walravens, W.; Maes, J.; Martins, J. C.; van Driessche, I.; Kovalenko, M. V.; Hens, Z. Highly dynamic ligand binding and light absorption coefficient of cesium lead bromide perovskite nanocrystals. *ACS Nano* **2016**, *10*, 2071−2081.
(39) Palazon, F.; Akkerman, Q. A.; Prato, M.; Manna, L. X-ray lithography on perovskite nanocrystals films: from patterning with anion-exchange reactions to enhanced stability in air and water. *ACS Nano* **2016**, *10*, 1224−1230.
(40) Li, J.; Yuan, X.; Jing, P.; Li, J.; Wei, M.; Hua, J.; Zhao, J.; Tian, L. Temperature-dependent photoluminescence of inorganic perovskite nanocrystal films. *RSC Adv.* **2016**, *6*, 78311−78316.
(41) Udayabhaskararao, T.; Kazes, M.; Houben, L.; Lin, H.; Oron, D. Nucleation, growth, and structural transformations of perovskite nanocrystals. *Chem. Mater.* **2017**, *29*, 1302−1308.
(42) Li, X.; Yu, D.; Cao, F.; Gu, Y.; Wei, Y.; Wu, Y.; Song, J.; Zeng, H. Healing all-inorganic perovskite films via recyclable dissolution−recrystallization for compact and smooth carrier channels of optoelectronic devices with high stability. *Adv. Funct. Mater.* **2016**, *26*, 5903−5912.

DOI: 10.1021/acsami.7b17432
ACS Appl. Mater. Interfaces 2018, 10, 5984−5991